Hydrodynamical approach to chirality production during axion inflation

E. V. Gorbar,[1,2] A. I. Momot,[1,*] O. O. Prikhodko,[1] and O. M. Teslyk[1]

[1]*Physics Faculty, Taras Shevchenko National University of Kyiv, 64/13, Volodymyrska Street, 01601 Kyiv, Ukraine*

[2]*Bogolyubov Institute for Theoretical Physics, 14-b, Metrolohichna Street, 03143 Kyiv, Ukraine*

(Received 17 November 2023; accepted 3 January 2024; published 31 January 2024)

We study chirality production in the pseudoscalar inflation model of magnetogenesis, taking into account the Schwinger effect and particle collisions in plasma in the relaxation time approximation. We consider the Schwinger production of one Dirac fermion species by an Abelian gauge field in two cases: (i) fermions carry only the weak charge with respect to the U(1) group and (ii) they are also charged with respect to another strongly coupled gauge group. While the gradient-expansion formalism is employed for the description of the evolution of the gauge field, plasma is described by a hydrodynamical approach, which allows us to determine the number, energy density, and chirality of produced fermions. It is found that, while chirality production is very efficient for both weakly and strongly interacting fermions, the resulting gauge field is typically stronger in the case of strongly interacting fermions, due to suppression of the Schwinger conductivity by particle collisions.

DOI: 10.1103/PhysRevD.109.023536

I. INTRODUCTION

The gamma-ray observations of blazars [1–4] imply the lower bound on the strength of the present large-scale magnetic fields B_0 given by $B_0 \gtrsim 10^{-16}$ G with coherence length possibly exceeding 1 Mpc. These observations strongly motivate the study of inflationary models of magnetogenesis because such models naturally explain the very large coherence length of generated magnetic fields [5–13].

Among various inflationary models of magnetogenesis, the axion inflation model is especially attractive because it produces maximally helical magnetic fields. This is an advantageous characteristic because the survival of helical magnetic fields is more efficient in the primordial plasma compared to the case of nonhelical magnetic fields [14]. The axion inflation model is characterized by the axial coupling of the inflaton field ϕ to the electromagnetic field by means of the interaction term $\beta\phi(\boldsymbol{E}\cdot\boldsymbol{B})/M_{\rm P}$, where $M_{\rm P}$ is the reduced Planck mass and β is the dimensionless coupling constant [15–33].

Obviously, in view of the chiral anomaly $\partial_\mu j^\mu_5 = e^2/(2\pi^2)(\boldsymbol{E}\cdot\boldsymbol{B})$, axion inflation inevitably leads to chirality production. In turn, nonzero chiral density via the chiral magnetic effect [34] affects the electromagnetic field evolution. Thus, axion inflation magnetogenesis implies a coupled evolutionary dynamics of the electromagnetic field and chirality.

A first step in the study of this joint evolution was done in Ref. [35], where it was found that chirality production is indeed very efficient, leading to the generation of a large chemical potential μ_5 at the end of axion inflation. To analyze the evolution of the electromagnetic field, the gradient-expansion formalism [28] was employed to account for the chiral magnetic effect (CME) [34] via an additional term $\boldsymbol{J}_{\rm CME} = e^2/(2\pi^2)\mu_5\boldsymbol{B}$ in the expression for the electric current. Such a contribution to the electric current is induced in chirally asymmetric ultrarelativistic fermion plasma in a magnetic field.

Reference [35] used the simple expressions for the electric conductivity σ induced by the Schwinger effect [36–38] in collinear electric and magnetic fields in de Sitter spacetime [30] and assumed that a local thermodynamic equilibrium was reached. According to the discussion in Ref. [30], such an assumption is questionable in the inflationary expanding Universe.

In the present paper, we extend the analysis performed in [35] in a few directions. First of all, we take into account the fact that the Schwinger induced current must be split into two contributions [24], where the first contribution originates from the lowest Landau level and, thus, corresponds to the chiral magnetic effect, while the second captures the contributions from higher Landau levels and is described by the usual Ohmic conductivity.

Second, we derive the Schwinger production rate Γ and fermion energy production rate Γ_ρ, which enter the

*momot.andriy@knu.ua

equations of motion for the fermion number and energy densities, taking into account the fact that the electric and magnetic fields generated during axion inflation are not completely collinear. However, performing a Lorentz boost, one can find an inertial frame where these fields are collinear. Then, using the expressions for Γ and Γ_ρ for collinear fields [39,40] and returning to the comoving reference frame, we obtain the corresponding expressions that account for noncollinearity of electric and magnetic fields generated during axion inflation.

The Schwinger effect [36–38] of charged particle-antiparticle pair production by a strong electric field is important for inflationary magnetogenesis because the generated electric fields are as strong as or even larger than the produced magnetic fields. We would like to note also that the energy production rate was not taken into account in [35]. However, the analysis in this paper has shown that it plays an important role for the evolution of plasma and electromagnetic fields. Finally, we have analyzed the impact of particle collisions on axion inflation magnetogenesis via the standard expression for the electric conductivity in the relaxation time approximation.

The paper is organized as follows. The axion inflation model is introduced in Sec. II. The gradient-expansion formalism is described in Sec. III. The set of equations for the evolution of plasma in the phenomenological hydrodynamical approach is derived in Sec. IV. The Schwinger pair and energy production rates are considered in Sec. V. The final set of equations is presented in Sec. VI. Numerical results for the chirality production and generated electromagnetic fields in the pseudoscalar inflation model are presented in Sec. VII. Section VIII is devoted to conclusions.

II. AXION INFLATION MODEL

In the axion inflation model, the inflaton field is represented by a pseudoscalar (axionlike) field ϕ that is coupled to an Abelian gauge field A_μ through the term of the Chern-Simons type. The corresponding action reads as

$$S = \int d^4x\sqrt{-g}\left[\frac{1}{2}g^{\mu\nu}\partial_\mu\phi\partial_\nu\phi - V(\phi) - \frac{1}{4}F_{\mu\nu}F^{\mu\nu} - \frac{1}{4}I(\phi)F_{\mu\nu}\tilde{F}^{\mu\nu} + \mathcal{L}_{\rm ch}(\chi, A_\mu)\right], \tag{1}$$

where $g = \det g_{\mu\nu}$ is the determinant of the spacetime metric, $V(\phi)$ is the inflaton potential, $I(\phi)$ is the axial coupling function, $F_{\mu\nu} = \partial_\mu A_\nu - \partial_\nu A_\mu$ is the gauge-field strength tensor, and

$$\tilde{F}^{\mu\nu} = \frac{1}{2\sqrt{-g}}\varepsilon^{\mu\nu\lambda\rho}F_{\lambda\rho} \tag{2}$$

is the corresponding dual tensor; $\varepsilon^{\mu\nu\lambda\rho}$ is the absolutely antisymmetric Levi-Civita symbol with $\varepsilon^{0123} = +1$. The last term in Eq. (1) is the Lagrangian for a generic matter field χ charged under the U(1) gauge group and, therefore, coupled to the gauge-field four-potential A_μ. For the sake of generality, we will not specify this term and assume that it describes all charged fields in the model.

Action (1) implies the following Euler-Lagrange equations for the inflaton and gauge field:

$$\frac{1}{\sqrt{-g}}\partial_\mu\left[\sqrt{-g}g^{\mu\nu}\partial_\nu\phi\right] + \frac{dV}{d\phi} + \frac{1}{4}\frac{dI}{d\phi}F_{\mu\nu}\tilde{F}^{\mu\nu} = 0, \tag{3}$$

$$\frac{1}{\sqrt{-g}}\partial_\mu\left[\sqrt{-g}F^{\mu\nu}\right] + \frac{dI}{d\phi}\tilde{F}^{\mu\nu}\partial_\mu\phi = j^\nu, \tag{4}$$

where

$$j^\nu = -\frac{\partial\mathcal{L}_{\rm ch}(\chi, A_\mu)}{\partial A_\nu} \tag{5}$$

is the electric four-current. Equation (4) should be supplemented by the Bianchi identity for the dual gauge-field strength tensor

$$\frac{1}{\sqrt{-g}}\partial_\mu\left[\sqrt{-g}\tilde{F}^{\mu\nu}\right] = 0. \tag{6}$$

The energy-momentum tensor equals

$$T_{\mu\nu} = \frac{2}{\sqrt{-g}}\frac{\delta S}{\delta g^{\mu\nu}} = \partial_\mu\phi\partial_\nu\phi - g^{\lambda\rho}F_{\mu\lambda}F_{\nu\rho} - g_{\mu\nu}\left[\frac{1}{2}\partial_\alpha\phi\partial^\alpha\phi - V(\phi) - \frac{1}{4}F_{\alpha\beta}F^{\alpha\beta}\right] + T^\chi_{\mu\nu}, \tag{7}$$

where the last term describes the contribution of charged matter fields.

The inflationary stage of the early Universe is characterized by the Friedmann-Lemaître-Robertson-Walker metric $g_{\mu\nu} = (1, -a^2(t), -a^2(t), -a^2(t))$, where $a(t)$ is the scale factor. Further, it is convenient to use in the analysis of inflationary magnetogenesis the temporal gauge for the vector potential A_μ, where $A_\mu = (0, -\boldsymbol{A})$. Then the three-vectors of electric $\boldsymbol{E} = (E^1, E^2, E^3)$ and magnetic $\boldsymbol{B} = (B^1, B^2, B^3)$ fields can be defined as $\boldsymbol{E} = -\frac{1}{a}\partial_0\boldsymbol{A}$ and $\boldsymbol{B} = \frac{1}{a^2}\mathrm{rot}\boldsymbol{A}$. They are physical fields measured by a comoving observer; therefore, we included the scale factor in their definition. The gauge-field stress tensor and its dual tensor are expressed in terms of electric and magnetic fields as follows:

$$F_{0i} = aE^i, \qquad F_{ij} = -a^2\varepsilon_{ijk}B^k, \qquad \tilde{F}_{0i} = aB^i, \qquad \tilde{F}_{ij} = a^2\varepsilon_{ijk}E^k. \tag{8}$$

The cosmic-expansion rate (the Hubble parameter $H = \dot{a}/a$) is determined by the Friedmann equation

$$H^2 = \frac{\rho}{3M_{\rm P}^2}, \tag{9}$$

where the total energy density ρ is given by the zero-zero component of the energy-momentum tensor (7),

$$\rho = T^0_0 = \left[\frac{1}{2}\dot{\phi}^2 + V(\phi)\right] + \frac{1}{2}\langle \boldsymbol{E}^2 + \boldsymbol{B}^2\rangle + \rho_{\rm c}. \tag{10}$$

Here the two terms in square brackets correspond to the energy density of the spatially homogeneous inflaton field, the next term describes the gauge-field contribution (angular brackets denote the vacuum expectation value), and the last term is the counterpart for the charged matter fields.

The electric four-current can be represented as

$$j^\mu = \left(\rho_{\rm ch}, \frac{1}{a}\boldsymbol{J}\right). \tag{11}$$

We assume that charged particles were absent in the Universe initially and were produced later in particle-antiparticle pairs via the Schwinger effect by a strong electric field connected with inflationary magnetogenesis. Therefore, we set the charge density to zero, $\rho_{\rm ch} = 0$. On the other hand, the current density three-vector $\boldsymbol{J}$ may be nonzero in the presence of the gauge field. Then the equations of motion (3), (4), and (6) take the following form in the three-vector notation:

$$\ddot{\phi} + 3H\dot{\phi} + V'(\phi) = I'(\phi)\langle \boldsymbol{E}\cdot\boldsymbol{B}\rangle, \tag{12}$$

$$\dot{\boldsymbol{E}} + 2H\boldsymbol{E} - \frac{1}{a}\mathrm{rot}\,\boldsymbol{B} + I'(\phi)\dot{\phi}\boldsymbol{B} + \boldsymbol{J} = 0, \tag{13}$$

$$\dot{\boldsymbol{B}} + 2H\boldsymbol{B} + \frac{1}{a}\mathrm{rot}\,\boldsymbol{E} = 0, \tag{14}$$

$$\mathrm{div}\,\boldsymbol{E} = 0, \qquad \mathrm{div}\,\boldsymbol{B} = 0. \tag{15}$$

Finally, to close the system of Maxwell's equations, we need to specify the electric current. We will show below that it can be represented in the form of the generalized Ohm's law,

$$\boldsymbol{J} = \sigma_E\boldsymbol{E} + \sigma_B\boldsymbol{B}, \tag{16}$$

where σ_E is the electric conductivity and σ_B is related to the chiral magnetic effect. We will derive expressions for these conductivities below. The Maxwell equation (13) takes the form

$$\dot{\boldsymbol{E}} + [2H + \sigma_E]\boldsymbol{E} + [I'(\phi)\dot{\phi} + \sigma_B]\boldsymbol{B} - \frac{1}{a}\mathrm{rot}\,\boldsymbol{B} = 0. \tag{17}$$

As mentioned in the Introduction, we employ the gradient-expansion formalism to solve the Maxwell equations in an inflating universe.

III. GRADIENT-EXPANSION FORMALISM

The gradient-expansion formalism proposed in Ref. [32] allows one to describe self-consistently the gauge-field production in the axial inflation model, including the Schwinger effect and the backreaction of produced particles on the gauge field. This method works in position space and, instead of vector quantities $\boldsymbol{E}$ and $\boldsymbol{B}$, operates with a set of scalar functions in a form of vacuum expectation values of scalar products of $\boldsymbol{E}$ and/or $\boldsymbol{B}$ with an arbitrary number of spatial derivatives (curls). These functions are

$$\mathcal{E}^{(n)} = \frac{1}{a^n}\langle \boldsymbol{E}\cdot\mathrm{rot}^n\boldsymbol{E}\rangle, \tag{18}$$

$$\mathcal{G}^{(n)} = -\frac{1}{2a^n}\langle \boldsymbol{E}\cdot\mathrm{rot}^n\boldsymbol{B} + (\mathrm{rot}^n\boldsymbol{B})\cdot\boldsymbol{E}\rangle, \tag{19}$$

$$\mathcal{B}^{(n)} = \frac{1}{a^n}\langle \boldsymbol{B}\cdot\mathrm{rot}^n\boldsymbol{B}\rangle. \tag{20}$$

Using Eqs. (14) and (17), we get the following equations of motion for bilinear electromagnetic functions:

$$\dot{\mathcal{E}}^{(n)} + [(n+4)H + 2\sigma_E]\mathcal{E}^{(n)} - 2[I'(\phi)\dot{\phi} + \sigma_B]\mathcal{G}^{(n)} + 2\mathcal{G}^{(n+1)} = [\dot{\mathcal{E}}^{(n)}]_{\rm b}, \tag{21}$$

$$\dot{\mathcal{G}}^{(n)} + [(n+4)H + \sigma_E]\mathcal{G}^{(n)} - [I'(\phi)\dot{\phi} + \sigma_B]\mathcal{B}^{(n)} - \mathcal{E}^{(n+1)} + \mathcal{B}^{(n+1)} = [\dot{\mathcal{G}}^{(n)}]_{\rm b}, \tag{22}$$

$$\dot{\mathcal{B}}^{(n)} + (n+4)H\mathcal{B}^{(n)} - 2\mathcal{G}^{(n+1)} = [\dot{\mathcal{B}}^{(n)}]_{\rm b}. \tag{23}$$

The right-hand sides of Eqs. (21)–(23) contain contributions due to boundary terms. Their necessity is dictated by the fact that the number of physically relevant modes (beyond the horizon) constantly grows during inflation. They have the following form:

$$[\dot{\mathcal{E}}^{(n)}]_{\rm b} = \frac{d\ln k_{\rm h}(t)}{dt}\frac{1}{4\pi^2}\left(\frac{k_{\rm h}(t)}{a(t)}\right)^{n+4}\sum_{\lambda=\pm1}\lambda^n E_\lambda(\xi_{\rm eff}(t), s(t)), \tag{24}$$

$$[\dot{\mathcal{G}}^{(n)}]_{\rm b} = \frac{d\ln k_{\rm h}(t)}{dt}\frac{1}{4\pi^2}\left(\frac{k_{\rm h}(t)}{a(t)}\right)^{n+4}\sum_{\lambda=\pm1}\lambda^{n+1} G_\lambda(\xi_{\rm eff}(t), s(t)), \tag{25}$$

$$[\dot{\mathcal{B}}^{(n)}]_{\rm b} = \frac{d\ln k_{\rm h}(t)}{dt}\frac{1}{4\pi^2}\left(\frac{k_{\rm h}(t)}{a(t)}\right)^{n+4}\sum_{\lambda=\pm1}\lambda^n B_\lambda(\xi_{\rm eff}(t), s(t)), \tag{26}$$

where $k_{\rm h}(t)$ is the momentum of a mode that is crossing the horizon at the moment of time t,

$$k_{\rm h}(t) = \max_{t'\le t}\left\{a(t')H(t')\left[|\xi_{\rm eff}(t')| + \sqrt{\xi^2_{\rm eff}(t') + s^2(t') + s(t')}\right]\right\}. \quad (27)$$

Here we introduced the following parameters:

$$\xi_{\rm eff}(t) = \frac{dI}{d\phi}\frac{\dot\phi}{2H} + \frac{\sigma_B(t)}{2H}, \qquad s(t) = \frac{\sigma_E(t)}{2H}. \quad (28)$$

The functions E_λ, G_λ, and B_λ were derived in Ref. [32] and have the form

$$E_\lambda(\xi_{\rm eff}, s) = \frac{e^{\pi\lambda\xi_{\rm eff}}}{r^2(\xi_{\rm eff}, s)}\Big|\big(ir(\xi_{\rm eff}, s) - i\lambda\xi_{\rm eff} - s\big) \times W_{-i\lambda\xi_{\rm eff},\frac{1}{2}+s}\big(-2ir(\xi_{\rm eff}, s)\big) + W_{1-i\lambda\xi_{\rm eff},\frac{1}{2}+s}\big(-2ir(\xi_{\rm eff}, s)\big)\Big|^2, \quad (29)$$

$$G_\lambda(\xi_{\rm eff}, s) = \frac{e^{\pi\lambda\xi_{\rm eff}}}{r(\xi_{\rm eff}, s)}\left\{\Re e\left[W_{i\lambda\xi_{\rm eff},\frac{1}{2}+s}\big(2ir(\xi_{\rm eff}, s)\big) \times W_{1-i\lambda\xi_{\rm eff},\frac{1}{2}+s}\big(-2ir(\xi_{\rm eff}, s)\big)\right] - s\left|W_{-i\lambda\xi_{\rm eff},\frac{1}{2}+s}\big(-2ir(\xi_{\rm eff}, s)\big)\right|^2\right\}, \quad (30)$$

$$B_\lambda(\xi_{\rm eff}, s) = e^{\pi\lambda\xi_{\rm eff}}\left|W_{-i\lambda\xi_{\rm eff},\frac{1}{2}+s}\big(-2ir(\xi_{\rm eff}, s)\big)\right|^2, \quad (31)$$

with $r(\xi_{\rm eff}, s) = |\xi_{\rm eff}| + \sqrt{\xi^2_{\rm eff} + s + s^2}$.

Note that the equation of motion for the nth order function always contains at least one function with the $(n+1)$th power of the curl. As a result, all equations are coupled into an infinite chain that needs to be truncated in practice. The easiest way to perform such a truncation is to express higher order quantities in terms of the lower order ones. For some maximal order $n_{\rm max}$, we impose the following conditions:

$$X^{(n_{\rm max}+1)} \approx \left(\frac{k_{\rm h}}{a}\right)^2 X^{(n_{\rm max}-1)} \quad (32)$$

for $X = \{\mathcal{E}, \mathcal{G}, \mathcal{B}\}$. This truncation rule respects transformation properties of $X^{(n)}$ under parity (i.e., relates either scalars or pseudoscalars). The truncation order $n_{\rm max}$ must be chosen in such a way that its further increase does not lead to a significant change of the result.

IV. HYDRODYNAMICAL DESCRIPTION OF PLASMA

To describe the dynamics of particles produced due to the Schwinger effect and their backreaction on the gauge field, we use the hydrodynamical approach and define the corresponding system of hydrodynamical equations in this section. Electromagnetohydrodynamics (EMHD) [41] is an extension of the familiar magnetohydrodynamics (MHD) [42] to the case where the displacement current and the generation of electromagnetic waves is important. Since the dynamics of the gauge field is definitely very important in the study of inflationary magnetogenesis, we adopt in this section the EMHD approach for the description of produced particles.

An important assumption of EMHD (as well as the more familiar MHD) is that the corresponding plasma is strongly collisional with the timescale of collisions shorter than the other characteristic times in the system. Certainly, the kinetic theory with its main ingredient in the form of the particle distribution function $f(\boldsymbol{p}, \boldsymbol{x}, t)$ in the phase space would provide a more accurate approach to the description of plasma; however, it is not easy to solve the corresponding Boltzmann equation. Therefore, although the hydrodynamical approach is more coarse and may sometimes miss the important physics, it is relatively simple because the hydrodynamical variables depend only on spacetime coordinates $\boldsymbol{x}$ and t. In addition, the hydrodynamical approach captures many of the important properties of plasma dynamics and is often qualitatively correct. Therefore, we use in the present paper the EMHD approach, paying special attention to the problem of attaining the collisional regime in our numerical analysis and leaving the implementation of the kinetic approach for future studies.

Since we consider a spatially uniform system with vanishing pressure and temperature gradients, we could set the hydrodynamical velocity $\boldsymbol{v}(\boldsymbol{x}, t)$ to zero. Then we are left with the following set of hydrodynamical variables that describe the plasma of chiral fermions (with negligibly small mass). These are the total number density of particles and antiparticles n, chirality density n_5, total energy density $\rho_{\rm c}$, and conduction current $\boldsymbol{j}_{\rm cond}$. Let us define now the set of equations that govern these hydrodynamical variables.

We begin with the equations of motion for the fermion number and energy densities. The Schwinger effect is characterized by the pair creation rate per unit volume and unit time Γ and the energy production rate per unit volume and unit time Γ_ρ, which will be specified in the next section. The equations of motion for the fermion number and energy densities have the following form:

$$\frac{dn}{dt} + 3Hn = 2\Gamma, \quad (33)$$

$$\frac{d\rho_{\rm c}}{dt} + 4H\rho_{\rm c} = \Gamma_\rho + (\boldsymbol{E}\cdot\boldsymbol{j}_{\rm cond}), \quad (34)$$

where terms with H take into account the redshift due to the Universe expansion. The first term on the right-hand side of Eq. (34) corresponds to the energy transfer from the gauge field to fermions due to the pair creation process, while the second term describes the increase of energy of produced particles in an external electric field. The former term can also be described as the scalar product of the electric field with some effective current—the so-called polarization current,

$$\Gamma_\rho = (\boldsymbol{E}\cdot\boldsymbol{j}_{\rm pol}). \tag{35}$$

Therefore, the equation of motion for the energy density can be rewritten as

$$\frac{d\rho_{\rm c}}{dt} + 4H\rho_{\rm c} = (\boldsymbol{E}\cdot\boldsymbol{J}), \tag{36}$$

where

$$\boldsymbol{J} = \boldsymbol{j}_{\rm pol} + \boldsymbol{j}_{\rm cond} \tag{37}$$

is the total electric current. Since we would like to combine the hydrodynamical approach with the gradient-expansion formalism, we represent the electric current in the form of the generalized Ohm's law

$$\boldsymbol{J} = \sigma_{E,\rm total}\boldsymbol{E} + \sigma_B\boldsymbol{B}. \tag{38}$$

Then

$$\sigma_{E,\rm total} = \sigma_E + \frac{\Gamma_\rho}{\langle \boldsymbol{E}^2\rangle}, \tag{39}$$

where the second term can be considered as the polarization conductivity. We will specify the explicit expressions for conductivities $\sigma_{E,B}$ below.

In order to write down the equation of motion for the chirality density, we note that the Schwinger pair production is insensitive to the chirality, i.e., it cannot produce the net chirality. However, since we have, in general, nonorthogonal electric and magnetic fields, the chiral anomaly leads to chirality production. Finally, the chirality flipping processes with the chirality flipping rate $\Gamma_{\rm flip}$ could lead to the equilibration of the chiral imbalance. Taking into account the above-mentioned effects, we find the following equation for the chirality density n_5:

$$\frac{dn_5}{dt} + 3Hn_5 = \frac{e^2}{2\pi^2}\langle \boldsymbol{E}\cdot\boldsymbol{B}\rangle - \Gamma_{\rm flip}n_5. \tag{40}$$

In the Standard Model, the chirality flipping rate $\Gamma_{\rm flip}$ is much less than the Hubble rate at temperatures above 80 TeV [43,44]; therefore, we will neglect these processes in what follows.

V. SCHWINGER PAIR AND ENERGY PRODUCTION RATES

In the previous section, we specified the equations that govern the temporal evolution of hydrodynamical variables. These equations depend on the Schwinger pair and energy production rates that we determine in this section. The Schwinger pair creation rate

$$\Gamma = \frac{1}{V}\frac{dN_{\rm pairs}}{dt} \tag{41}$$

is a Lorentz scalar and the energy production rate

$$\Gamma_\rho = \frac{1}{V}\frac{dW}{dt} \tag{42}$$

transforms as the zeroth component of a contravariant four-vector.

As mentioned in the Introduction, although electric and magnetic fields generated during axion inflation are not completely collinear, performing a Lorentz boost one can find an inertial frame where these fields are collinear. Then, following the analysis in [39,40], one can easily calculate the Schwinger number and energy production rates in that frame and return back to the initial frame performing the corresponding Lorentz boost. This procedure allows us to take into account noncollinearity of electric and magnetic fields generated during axion inflation. Obviously, such a procedure implicitly assumes that the spatial dependence of electric and magnetic fields can be neglected.

The calculation of the Schwinger number and energy production rates in the reference frame where electric and magnetic fields are collinear is straightforward (we denote electric and magnetic fields in this reference frame with tilde). Then the production rates can be computed using the semiclassical approximation. For the Dirac fermion with mass m, the Schwinger pair production process can be regarded as quantum tunneling through the energy gap between the upper and lower continua. In the presence of constant and collinear electric and magnetic fields directed along the z axis, the semiclassical energy of the fermion has the form

$$\mathcal{E}_\pm = |e\tilde{E}|z \pm \sqrt{p_z^2 + 2|e\tilde{B}|\left(n + \frac{1}{2} + \hat{\sigma}\right) + m^2}, \tag{43}$$

where $n = 0, 1, 2, \ldots$ is the Landau level number, $\hat{\sigma} = \pm\frac{1}{2}$ is the spin projection on the z axis, and p_z is the continuous momentum along the z axis. A fermion with energy $\mathcal{E}$ and given values of n and $\hat{\sigma}$ can propagate in the regions of space where p_z is real. However, there is a finite region where p_z can be only imaginary, which is the classically forbidden region. The tunneling probability is proportional to [39,40]

$$\mathcal{P} \propto \exp\left(-2\int_{z_-}^{z_+} |p_z| dz\right) = \exp\left(-\pi \frac{2|e\tilde{B}|(n+\frac{1}{2}+\hat{\sigma})+m^2}{|e\tilde{E}|}\right), \quad (44)$$

where $z_\pm$ are classical turning points. This expression gives the probability of the pair production at the nth Landau level with the spin projection $\hat{\sigma}$. Following Ref. [40], we can use it to compute the pair and energy production rates. For simplicity, let us consider fermions with vanishing mass.[1] Then we get

$$\begin{aligned}\Gamma &= \frac{|e\tilde{E}||e\tilde{B}|}{4\pi^2}\sum_{n,\hat{\sigma}} \exp\left(-\pi\frac{2|e\tilde{B}|(n+\frac{1}{2}+\hat{\sigma})}{|e\tilde{E}|}\right) \\ &= \frac{|e\tilde{E}||e\tilde{B}|}{4\pi^2}\left[1+2\sum_{k=1}^{\infty} e^{-2\pi\frac{|\tilde{B}|}{|\tilde{E}|}k}\right] \\ &= \frac{|e\tilde{E}||e\tilde{B}|}{4\pi^2}\coth\left(\pi\frac{|\tilde{B}|}{|\tilde{E}|}\right), \end{aligned} \quad (45)$$

$$\begin{aligned}\tilde{\Gamma}_\rho &= \frac{|e\tilde{E}||e\tilde{B}|}{4\pi^2}\sum_{n,\hat{\sigma}} 2\sqrt{2|e\tilde{B}|\left(n+\frac{1}{2}+\hat{\sigma}\right)} \\ &\quad\times \exp\left(-\pi\frac{2|e\tilde{B}|(n+\frac{1}{2}+\hat{\sigma})}{|e\tilde{E}|}\right) \\ &= \frac{|e\tilde{E}||e\tilde{B}|}{4\pi^2} 4\sqrt{2|e\tilde{B}|}\sum_{k=1}^{\infty}\sqrt{k}\, e^{-2\pi\frac{|\tilde{B}|}{|\tilde{E}|}k} \\ &= \frac{|e\tilde{E}||e\tilde{B}|^{3/2}\sqrt{2}}{\pi^2}\mathrm{Li}_{-\frac{1}{2}}\left(e^{-2\pi\frac{|\tilde{B}|}{|\tilde{E}|}}\right), \end{aligned} \quad (46)$$

where $\mathrm{Li}_{-\frac{1}{2}}$ is the polylogarithm of order $-\frac{1}{2}$. In the second expression, factor $2\sqrt{2|e\tilde{B}|(n+\frac{1}{2}+\hat{\sigma})}$ is the energy difference between the positive and negative energy continua at fixed z.

As stated above, electric $\boldsymbol{E}$ and magnetic $\boldsymbol{B}$ fields generated during axion inflation are, in general, not collinear. Let us assume without loss of generality that $\boldsymbol{E}$ and $\boldsymbol{B}$ in the comoving frame lie in the xOy plane. Then the velocity of boost leading to the collinear frame is parallel to the z axis and equal to

$$\boldsymbol{v} = \frac{2[\boldsymbol{E}\times\boldsymbol{B}]}{\boldsymbol{E}^2+\boldsymbol{B}^2+\sqrt{(\boldsymbol{E}^2-\boldsymbol{B}^2)^2+4(\boldsymbol{E}\cdot\boldsymbol{B})^2}}. \quad (47)$$

[1]The mass can be neglected if $m^2 \ll |e\tilde{E}|$, which is typically satisfied during inflation. In the opposite case, the Schwinger pair production is exponentially suppressed and, therefore, is not interesting for the present study.

The corresponding Lorentz factor is given by

$$\gamma = \frac{1}{\sqrt{1-v^2}} = \frac{1}{\sqrt{2}}\left[1+\frac{\boldsymbol{E}^2+\boldsymbol{B}^2}{\sqrt{(\boldsymbol{E}^2-\boldsymbol{B}^2)^2+4(\boldsymbol{E}\cdot\boldsymbol{B})^2}}\right]^{1/2}. \quad (48)$$

The resulting values of electric and magnetic fields in the collinear frame can be easily found from the invariants of the gauge-field tensor, which are the same in both frames,

$$\mathcal{I}_1 = \frac{1}{2}F_{\mu\nu}F^{\mu\nu} = \boldsymbol{B}^2-\boldsymbol{E}^2 = \tilde{B}^2-\tilde{E}^2, \quad (49)$$

$$\mathcal{I}_2 = -\frac{1}{4}F_{\mu\nu}\tilde{F}^{\mu\nu} = \boldsymbol{E}\cdot\boldsymbol{B} = \tilde{E}\,\tilde{B}, \quad (50)$$

which gives

$$\tilde{E} = \frac{1}{\sqrt{2}}\left[\boldsymbol{E}^2-\boldsymbol{B}^2+\sqrt{(\boldsymbol{E}^2-\boldsymbol{B}^2)^2+4(\boldsymbol{E}\cdot\boldsymbol{B})^2}\right]^{1/2}, \quad (51)$$

$$\tilde{B} = \mathrm{sign}(\boldsymbol{E}\cdot\boldsymbol{B})\frac{1}{\sqrt{2}}\left[\boldsymbol{B}^2-\boldsymbol{E}^2+\sqrt{(\boldsymbol{E}^2-\boldsymbol{B}^2)^2+4(\boldsymbol{E}\cdot\boldsymbol{B})^2}\right]^{1/2}. \quad (52)$$

Note that $\tilde{E}$ is defined as a positive quantity, while the projection of magnetic field on the direction of electric field $\tilde{B}$ may have any sign, depending on the scalar product $\boldsymbol{E}\cdot\boldsymbol{B}$ in the comoving frame.

Finally, expressing everything in terms of gauge fields in the comoving frame, we obtain the sought expression for the pair production rate per unit volume and unit time,

$$\begin{aligned}\Gamma &= \frac{e^2|\boldsymbol{E}\cdot\boldsymbol{B}|}{4\pi^2}\coth\frac{2\pi|\boldsymbol{E}\cdot\boldsymbol{B}|}{\boldsymbol{E}^2-\boldsymbol{B}^2+\Delta}, \\ \Delta &= \sqrt{(\boldsymbol{E}^2-\boldsymbol{B}^2)^2+4(\boldsymbol{E}\cdot\boldsymbol{B})^2}. \end{aligned} \quad (53)$$

The energy production rate in the comoving frame can be found by performing the inverse Lorentz boost and is given by

$$\begin{aligned}\Gamma_\rho &= \gamma\tilde{\Gamma}_\rho = \frac{e^{5/2}|\boldsymbol{E}\cdot\boldsymbol{B}|}{2^{1/4}\pi^2}\frac{(\boldsymbol{E}^2+\boldsymbol{B}^2+\Delta)^{1/2}(\boldsymbol{B}^2-\boldsymbol{E}^2+\Delta)^{1/4}}{\Delta^{1/2}} \\ &\quad\times\mathrm{Li}_{-\frac{1}{2}}\left(e^{-\frac{4\pi|\boldsymbol{E}\cdot\boldsymbol{B}|}{\boldsymbol{E}^2-\boldsymbol{B}^2+\Delta}}\right) \\ &= \frac{e^{5/2}2^{1/4}}{\pi^2}\frac{(\boldsymbol{E}^2+\boldsymbol{B}^2+\Delta)^{1/2}}{\Delta^{1/2}(\boldsymbol{E}^2-\boldsymbol{B}^2+\Delta)^{1/4}}|\boldsymbol{E}\cdot\boldsymbol{B}|^{3/2} \\ &\quad\times\mathrm{Li}_{-\frac{1}{2}}\left(e^{-\frac{4\pi|\boldsymbol{E}\cdot\boldsymbol{B}|}{\boldsymbol{E}^2-\boldsymbol{B}^2+\Delta}}\right). \end{aligned} \quad (54)$$

Before proceeding to numerical analysis, it is useful to collect everything and present the final set of equations.

VI. FINAL SET OF EQUATIONS

The system of equations governing the joint evolution of the inflaton field, gauge field, and produced plasma has the following form:

(i) the Friedmann equation for the Hubble rate

$$H^2=\left(\frac{\dot{a}}{a}\right)^2=\frac{1}{3M_{\rm P}^2}\left[\frac{1}{2}\dot{\phi}^2+V(\phi)+\frac{1}{2}\left(\mathcal{E}^{(0)}+\mathcal{B}^{(0)}\right)+\rho_{\rm c}\right], \tag{55}$$

(ii) the Klein-Gordon equation for the inflaton field

$$\ddot{\phi}+3H\dot{\phi}+V'(\phi)=-I'(\phi)\mathcal{G}^{(0)}, \tag{56}$$

(iii) the gradient-expansion formalism equations for the gauge-field bilinear functions

$$\dot{\mathcal{E}}^{(n)}+\left[(n+4)H+2\sigma_E+2\frac{\Gamma_\rho}{\mathcal{E}^{(0)}}\right]\mathcal{E}^{(n)}-2[I'(\phi)\dot{\phi}+\sigma_B]\mathcal{G}^{(n)}+2\mathcal{G}^{(n+1)}=\frac{d\ln k_{\rm h}(t)}{dt}\frac{1}{4\pi^2}\left(\frac{k_{\rm h}(t)}{a(t)}\right)^{n+4}\times\sum_{\lambda=\pm1}\lambda^n E_\lambda\left(\xi_{\rm eff}(t),s(t)\right), \tag{57}$$

$$\dot{\mathcal{G}}^{(n)}+\left[(n+4)H+\sigma_E+\frac{\Gamma_\rho}{\mathcal{E}^{(0)}}\right]\mathcal{G}^{(n)}-[I'(\phi)\dot{\phi}+\sigma_B]\mathcal{B}^{(n)}-\mathcal{E}^{(n+1)}+\mathcal{B}^{(n+1)}=\frac{d\ln k_{\rm h}(t)}{dt}\frac{1}{4\pi^2}\left(\frac{k_{\rm h}(t)}{a(t)}\right)^{n+4}\times\sum_{\lambda=\pm1}\lambda^{n+1}G_\lambda\left(\xi_{\rm eff}(t),s(t)\right), \tag{58}$$

$$\dot{\mathcal{B}}^{(n)}+(n+4)H\mathcal{B}^{(n)}-2\mathcal{G}^{(n+1)}=\frac{d\ln k_{\rm h}(t)}{dt}\frac{1}{4\pi^2}\left(\frac{k_{\rm h}(t)}{a(t)}\right)^{n+4}\times\sum_{\lambda=\pm1}\lambda^n B_\lambda\left(\xi_{\rm eff}(t),s(t)\right), \tag{59}$$

where

$$\xi_{\rm eff}(t)=\frac{dI}{d\phi}\frac{\dot{\phi}}{2H}+\frac{\sigma_B}{2H},\qquad s(t)=\frac{\sigma_E+\Gamma_\rho/\mathcal{E}^{(0)}}{2H}, \tag{60}$$

(iv) the equation for the fermion energy density

$$\frac{d\rho_{\rm c}}{dt}+4H\rho_{\rm c}=\Gamma_\rho+\sigma_E\mathcal{E}^{(0)}-\sigma_B\mathcal{G}^{(0)}, \tag{61}$$

(v) the equation for the fermion chirality density

$$\frac{dn_5}{dt}+3Hn_5=-\frac{e^2}{2\pi^2}\mathcal{G}^{(0)}, \tag{62}$$

(vi) the equation for the fermion number density

$$\frac{dn}{dt}+3Hn=2\Gamma. \tag{63}$$

Here

$$\Gamma=\frac{e^2|\mathcal{G}^{(0)}|}{4\pi^2}\coth\frac{2\pi|\mathcal{G}^{(0)}|}{\mathcal{E}^{(0)}-\mathcal{B}^{(0)}+\Delta}, \tag{64}$$

$$\Gamma_\rho=\frac{e^{5/2}2^{1/4}}{\pi^2}\frac{(\mathcal{E}^{(0)}+\mathcal{B}^{(0)}+\Delta)^{1/2}}{\Delta^{1/2}(\mathcal{E}^{(0)}-\mathcal{B}^{(0)}+\Delta)^{1/4}}\times|\mathcal{G}^{(0)}|^{3/2}{\rm Li}_{-\frac{1}{2}}\left(e^{-\frac{4\pi|\mathcal{G}^{(0)}|}{\mathcal{E}^{(0)}-\mathcal{B}^{(0)}+\Delta}}\right), \tag{65}$$

with

$$\Delta=\sqrt{(\mathcal{E}^{(0)}-\mathcal{B}^{(0)})^2+4(\mathcal{G}^{(0)})^2}. \tag{66}$$

Finally, for conductivities, we take the expressions from Ref. [24], see Eqs. (4.11) and (4.12),

$$\sigma_E=\frac{e^3}{3\pi^2H}\frac{\sqrt{\mathcal{B}^{(0)}}}{\exp\left(2\pi\sqrt{\frac{\mathcal{B}^{(0)}}{\mathcal{E}^{(0)}}}\right)-1}, \tag{67}$$

$$\sigma_B=-\frac{e^3}{6\pi^2H}\sqrt{\mathcal{E}^{(0)}}{\rm sign}(\mathcal{G}^{(0)}). \tag{68}$$

As we discussed in Sec. IV, the hydrodynamical approach implies that plasma is in the collisional regime with the timescale of collisions shorter than the other characteristic times in the system. The characteristic timescale of collisions τ of charged fermions in plasma at thermal equilibrium with temperature T can be estimated as [45,46]

$$\tau_{\rm eq}=\frac{c_0}{T\left(\frac{e^2}{4\pi}\right)^2\ln|e|^{-1}}, \tag{69}$$

where $e = \sqrt{4\pi\alpha_w} \approx 0.35$ is the gauge charge[2] and c_0 is a dimensionless constant of order unity.[3]

Equation (69) can be used for the system in the state of thermodynamic equilibrium, in which the temperature can be introduced. In the beginning of inflation, the system is definitely not in the equilibrium state and it is not obvious that it will come to equilibrium at the end of inflation. On the other hand, collisions still may play an important role during inflation. To deal with such a case, instead of Eq. (69), we can estimate the collision time for charged particles as follows:

$$\tau_p = \frac{\rho_c^2}{ke^4 \ln(e^{-1}) n^3}, \tag{70}$$

where k is a model-dependent factor that accounts for the number of charged particle species and their interaction strength. In our analysis, we consider the two limiting cases $k = 1$ (for example, it could be a single lepton interacting only via electroweak interactions in the Standard Model) and $k = 10^4$. The latter can be considered as the case of strongly interacting particles, e.g., quarks in the Standard Model, where k equals the product of the number of quark species N_q and the square of the ratio of the strong and weak coupling constants $(\alpha_s/\alpha_w)^2$. Clearly, factor k is quite model dependent because neither the number of particle species nor their interaction strength are fixed at the Hubble scale of inflation. Therefore, our choice of two numerical values of k is by no means definite, but serves only for illustrative purposes.

We would also like to note that, while the gradient-expansion method we use is based on the approximation of homogeneous axion, it is known that including axion inhomogeneity quantitatively changes the behavior in the strong backreaction regime [47,48]. In the weakly interacting fermion case, the analysis performed in [47,48] should stay mainly intact, as particle collisions should not change much the results obtained in these papers. On the other hand, it is not immediately clear what happens in the case where fermions interact strongly with other gauge fields. Strong interaction results in more efficient equilibration in the fermion sector and smoothing its inhomogeneity. This suggests that inhomogeneities in the gauge and axion sectors should be weakened too. Still, the dynamics in the strongly interacting case is inherently nonlinear; therefore, definite conclusions on this question could be drawn only via analyses like in [47,48] extended to the case of strongly interacting fermions.

If the collision time is less than Hubble time $\tau_H \simeq 1/H$, then the expressions for conductivities can be modified by replacing $1/(3H)$ with the collision time τ_p [24],

$$\sigma_E = \frac{e^3\tau_p}{\pi^2} \frac{\sqrt{\mathcal{B}^{(0)}}}{\exp\left(2\pi\sqrt{\frac{\mathcal{B}^{(0)}}{\mathcal{E}^{(0)}}}\right) - 1}, \tag{71}$$

$$\sigma_B = -\frac{e^3\tau_p}{2\pi^2}\sqrt{\mathcal{E}^{(0)}}\,\mathrm{sign}(\mathcal{G}^{(0)}). \tag{72}$$

Having presented the complete system of equations, we proceed now to its numerical analysis.

VII. NUMERICAL ANALYSIS

We consider two potentials for the inflaton field in our analysis. The first is the α-attractor inflation potential

$$V(\phi) = V_0 \mathrm{th}^2\left(\frac{\phi}{\sqrt{6\alpha}M_P}\right), \tag{73}$$

with $\alpha = 1$ and $V_0 = 10^{-10}M_P^4$, and the second is the quadratic potential

$$V(\phi) = \frac{m_\phi^2\phi^2}{2}, \tag{74}$$

with $m_\phi = 6 \times 10^{-6}M_P$. The amplitudes of both potentials were chosen from the requirement that they imply the correct amplitude of the curvature power spectrum constrained by the cosmic microwave background (CMB) observations [49].[4] The axial coupling function has the simplest linear form for both potentials,

$$I(\phi) = \frac{\beta\phi}{M_P}, \tag{75}$$

where β is the dimensionless coupling constant typically varying in the range 10–30.

The initial conditions for the inflaton and its derivative are given by

[2]Here we used the value of the Standard Model hypercharge coupling constant g' at the energy scale of the Z-boson mass, $m_Z = 91.2$ GeV. If view of the coupling constant running with momentum, a better choice would be to take the value of the hypercharge coupling constant at the Hubble scale. However, the latter is model dependent, hence, the collision time is a model-dependent quantity too.

[3]In general, it depends on particle's momentum; however, for simplicity, we will neglect this dependence and assume it to be constant. Its numerical value also depends on the number of charged degrees of freedom in plasma. We will keep it as a free parameter that determines the intensity of collisions in plasma.

[4]Here we disregard the fact that the quadratic inflaton potential (74) is strongly disfavored by the CMB observations [49] and use it for illustrative purposes. Moreover, in many viable inflationary models, when the inflaton approaches the minimum of its potential, the latter can be well approximated by the ϕ^2 term.

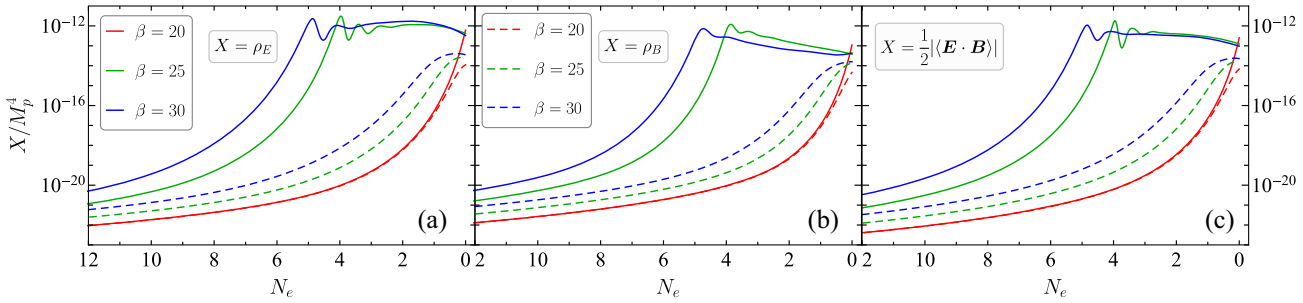

FIG. 1. The electric energy density ρ_E (a), magnetic energy density ρ_B (b), and Chern-Pontryagin density $\frac{1}{2}|\langle \boldsymbol{E} \cdot \boldsymbol{B} \rangle|$ (c) as functions of the number of e-foldings counted from the end of inflation N_e for the α-attractor potential (73) and three different values of the axial coupling parameter $\beta = 20$ (red lines), $\beta = 25$ (green lines), and $\beta = 30$ (blue lines). The dependence for weakly interacting particles ($k = 1$) is shown by dashed lines and by solid lines for strongly interacting particles ($k = 10^4$).

$$\phi(0) = 6.25 M_{\rm P},$$
$$\dot{\phi}(0) = -\frac{M_{\rm P} V'(\phi_0)}{\sqrt{3V(\phi_0)}} \approx -1.13 \times 10^{-7} M_{\rm P}^2, \qquad (76)$$

for potential (73) and

$$\phi(0) = 15.55 M_{\rm P},$$
$$\dot{\phi}(0) = -\frac{M_{\rm P} V'(\phi_0)}{\sqrt{3V(\phi_0)}} \approx -4.9 \times 10^{-6} M_{\rm P}^2, \qquad (77)$$

for potential (74), where the inflaton initial value allows us to get at least $60e$-foldings of inflation and the value of its initial derivative is computed assuming the slow-roll approximation. Note that only the last $10 - 15e$-foldings are important for magnetogenesis and fermion production; however, the initial conditions should be specified well before this moment. The initial conditions for gauge-field bilinear functions, energy density, chirality density, and the number density of produced particles are set to zero.

Our numerical analysis revealed that the Hubble time is much less than the collision time $\tau_H \ll \tau_{\rm p}$ for weakly interacting particles during the whole inflation; hence, the corresponding plasma is in the collisionless regime and the expressions for conductivities (67) and (68) should be applied. For strongly interacting particles, vice versa, the collision time is much less than the Hubble time $\tau_H \gg \tau_{\rm p}$ during inflation, i.e., this plasma in the collision regime; hence, the expressions for conductivities (71) and (72) should be used throughout the whole inflation.

The results of calculations for the α-attractor potential (73) are presented in Figs. 1–3 and for quadratic potential (74) in Figs. 4–6. The most general results of our analysis could be summarized as follows. According to Figs. 1, 2(a), 4, and 5(a), as one could expect, the generated electric, magnetic, Chern-Pontryagin, and fermion number densities at a given value of β are larger for strongly interacting particles compared to the case of weakly interacting particles because smaller collision time reduces the conduction electric current that tends to screen the electric field. This makes generated electromagnetic fields stronger. On the other hand, no such universal conclusion could be drawn for the generated fermion energy density as Figs. 3 and 6 imply. As to chiral asymmetry $(n - n_5)/n$, its value at the end of inflation at a given value of β, like the value of generated electromagnetic fields, is larger for strongly interacting particles compared to the case of weakly interacting particles.

As to the role of the axial coupling constant β, Figs. 1–6 demonstrate a nonmonotonic dependence of the generated

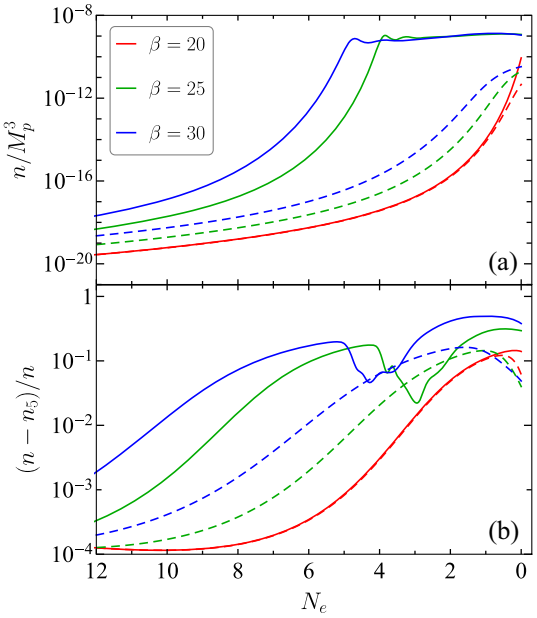

FIG. 2. The total number density n (a) and chiral asymmetry $(n - n_5)/n$ (b) as a function of the number of e-foldings counted from the end of inflation N_e for the α-attractor potential (73) and three different values of the axial coupling parameter $\beta = 20$ (red lines), $\beta = 25$ (green lines), and $\beta = 30$ (blue lines). The dependence for weakly interacting particles ($k = 1$) is shown by dashed lines and by solid lines for strongly interacting particles ($k = 10^4$).

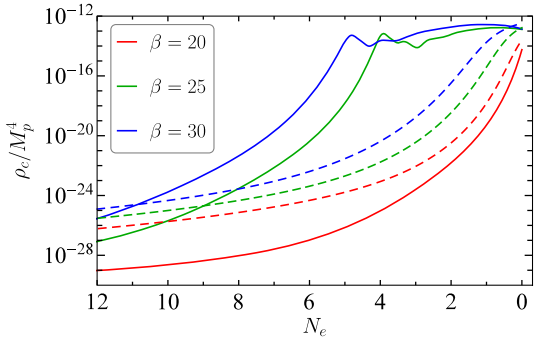

FIG. 3. The dependence of the fermion energy density ρ_c on the number of e-foldings counted from the end of inflation N_e in the case of the α-attractor potential (73) and three values of the axial coupling parameter $\beta = 20$ (red lines), $\beta = 25$ (green lines), $\beta = 30$ (blue lines). The dependence for weakly interacting particles ($k = 1$) is shown by dashed lines and by solid lines for strongly interacting particles ($k = 10^4$).

electromagnetic fields, fermion number and energy densities, and chiral asymmetry on the number of e-foldings N_e from the end of inflation for a sufficiently large value of the axial coupling constant β.

Comparing Figs. 1–3 and 4–6 plotted for the α-attractor and quadratic potentials, respectively, we see that the corresponding results are rather similar, i.e., the characteristics of generated electromagnetic fields and chiral asymmetry do not show a significant dependence on the form of the inflaton potential.

Let us provide more detailed quantitative information on the obtained results. For weakly interacting particles in the case of the α-attractor potential (73), the increase of coupling constant β from 20 to 30 results in the increase of the electric- and magnetic-field energy densities and Chern-Pontryagin density $\frac{1}{2}|\langle \boldsymbol{E}\cdot\boldsymbol{B}\rangle|$ (see Fig. 1), as well as in the increase of the fermion number (see Fig. 2) and energy densities (see Fig. 3). The chiral asymmetry $(n - n_5)/n$ is equal to 0.062, 0.040, and 0.049 for $\beta = 20$, 25, and 30, respectively; i.e., it is not monotonic as β changes.

For strongly interacting particles, where the collisional regime is realized due to strong interactions, the magnitude of the considered densities is more than 10 times larger than that in the case of weakly interacting particles. In addition, chiral asymmetry increases to 0.14, 0.29, and 0.38 and is monotonic with β. Moreover, qualitative changes in the time evolution are observed for $\beta = 25$ and 30, namely, a nonmonotonic behavior due to the backreaction of produced gauge fields. Indeed, while the highest value of the magnetic energy density is observed for $\beta = 15$, the other considered quantities reach their highest values for $\beta = 20$. The largest value of chiral asymmetry is 0.57.

For the quadratic potential (74), the increase of β from 10 to 25 also leads to the increase of ρ_E, ρ_B as well as $\frac{1}{2}|\langle \boldsymbol{E}\cdot\boldsymbol{B}\rangle|$, n, and ρ_c (see Figs. 4–6). The most considerable growth is observed between $\beta = 10$ and 15. The value of $(n - n_5)/n$ is in the range from 0.095 to 0.15.

Concerning magnetogenesis, the important issue in its study is to determine how magnetic fields generated during inflation evolve through the sequence of cosmological epochs until the present. After the end of inflation, the preheating takes place when the inflaton field oscillates in the potential minimum and decays into different particles. Although the electromagnetic field could be amplified during the preheating stage due to the interaction with the rapidly oscillating inflaton, e.g., through the mechanism of parametric resonance, for simplicity, we could assume that the magnetic field is not enhanced during the preheating stage.

Further, after reheating, the plasma of created particles thermalizes and the Universe enters its hot radiation dominated phase. If the turbulent regime does not take place, then the magnetic field evolves adiabatically, i.e., the corresponding comoving quantity remains constant,

$$\tilde{B}(t_{\rm reh}) = \tilde{B}(t) = B(t)\left(\frac{a_0}{a_e}\right)^{-2}, \tag{78}$$

where a is the scale factor. The analysis in Sec. VII of [28] defines the ratio of scaling factors a_0/a_e and gives the present day value of the magnetic field

$$B_0 \simeq 4\times 10^{-15}\ \mathrm{G}\left(\frac{T_{\rm reh}}{10^{14}\ \mathrm{GeV}}\right)^{-1/3}. \tag{79}$$

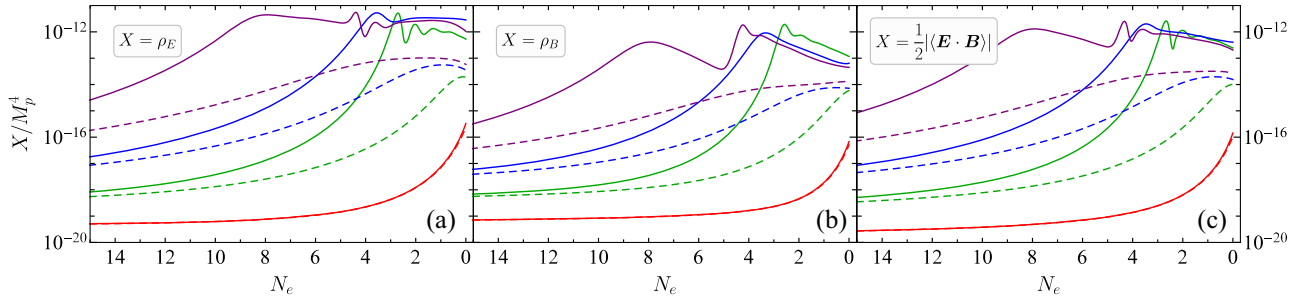

FIG. 4. The electric energy density ρ_E (a), magnetic energy density ρ_B (b), and Chern-Pontryagin density $\frac{1}{2}|\langle \mathbf{E}\cdot\mathbf{B}\rangle|$ (c) as functions of the number of e-foldings counted from the end of inflation N_e for the quadratic potential (74) and four values of the axial coupling parameter $\beta = 10$ (red lines), $\beta = 15$ (green lines), $\beta = 20$ (blue lines), $\beta = 25$ (purple lines). The dependence for weakly interacting particles ($k = 1$) is shown by dashed lines and by solid lines for strongly interacting particles ($k = 10^4$).

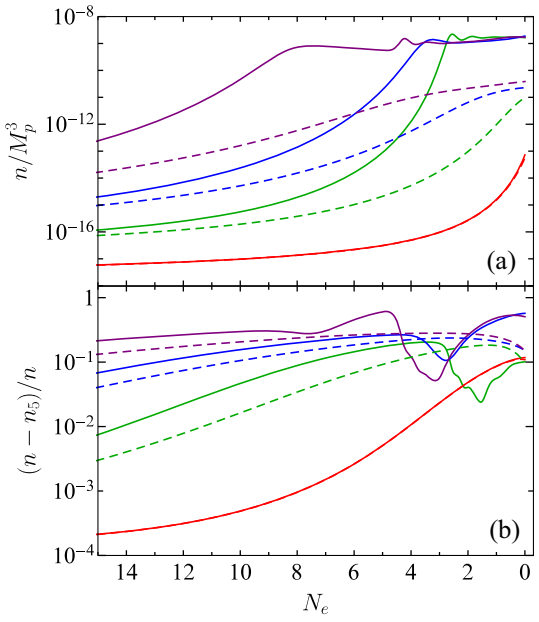

FIG. 5. The total number density n (a) and chiral asymmetry $(n-n_5)/n$ (b) as a function of the number of e-foldings counted from the end of inflation N_e for the quadratic potential (74) and four different values of the axial coupling parameter $\beta = 10$ (red lines), $\beta = 15$ (green lines), $\beta = 20$ (blue lines), $\beta = 25$ (purple lines). The dependence for weakly interacting particles $(k = 1)$ is shown by dashed lines and by solid lines for strongly interacting particles $(k = 10^4)$.

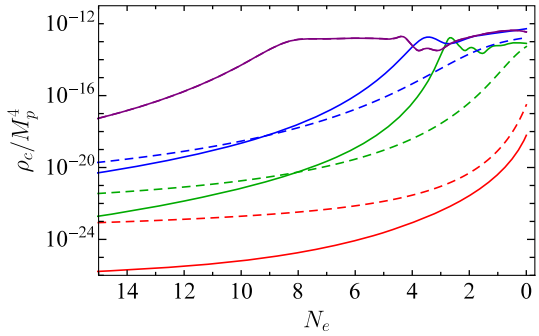

FIG. 6. The same dependences as shown in Fig. 3 for the quadratic potential (74) and four different values of the axial coupling parameter $\beta = 10$ (red lines), $\beta = 15$ (green lines), $\beta = 20$ (blue lines), $\beta = 25$ (purple lines).

VIII. SUMMARY

Our analysis of chirality production and its impact on generated electromagnetic fields during axion inflation via the gradient-expansion formalism and hydrodynamical approach (taking into account particle collisions in the relaxation time approximation) in the gauge-field and fermion sectors, respectively, led to the following results.

Comparing the particle collision time with the Hubble time, we found that local thermodynamic equilibrium is not reached for weakly interacting particles equilibrating only via the electroweak interactions and a realistically small number of particle species. However, for strongly interacting particles, the characteristic collision time appears to be much smaller than the Hubble time. Although the intense particle production due to the Schwinger effect may still prevent the system from reaching the state of local thermodynamic equilibrium, the particle collisions may have a strong impact on the pair production process and, consequently, on the outcome of magnetogenesis during pseudoscalar inflation.

We found that the generated electric, magnetic, Chern-Pontryagin, and fermion number densities at a given value of the coupling constant β are larger for strongly interacting particles compared to the case of weakly interacting particles, as one could expect, because smaller collision time reduces the conduction electric current, which tends to decrease the electric field. Therefore, generated electromagnetic fields are stronger. Although the value of produced chiral asymmetry at the end of inflation at fixed β is larger for strongly interacting particles compared to the case of weakly interacting particles, chiral asymmetry can be larger for weakly interacting particles for a few e-foldings close to the end of inflation. For a sufficiently large value of the axial coupling constant β, a nonmonotonic dependence of generated electromagnetic fields, fermion number and energy densities, and chiral asymmetry on the number of e-foldings is observed near the end of inflation due to the strong backreaction of produced gauge fields. In addition, the obtained results show that the values of generated electromagnetic fields and chiral asymmetry do not depend notably on the form of the inflaton potential.

We would like to note that the present study allows us to draw only some general qualitative conclusions about chirality production during axion inflation and does not claim to provide an accurate quantitative description of the process. The latter could be realized only in the framework of the chiral kinetic theory with a realistic collision integral describing the interaction processes in plasma. We plan to address this issue elsewhere.

ACKNOWLEDGMENTS

The authors are grateful to S. I. Vilchinskii for useful discussions and participation in the early stage of this project. The work of E. V. G., A. I. M., and O. M. T. was supported by the National Research Foundation of Ukraine Project No. 2020.02/0062.

[1] A. Neronov and I. Vovk, Evidence for strong extragalactic magnetic fields from Fermi observations of TeV blazars, Science **328**, 73 (2010).
[2] A. M. Taylor, I. Vovk, and A. Neronov, Extragalactic magnetic fields constraints from simultaneous GeV-TeV observations of blazars, Astron. Astrophys. **529**, A144 (2011).
[3] F. Tavecchio, G. Ghisellini, L. Foschini, G. Bonnoli, G. Ghirlanda, and P. Coppi, The intergalactic magnetic field constrained by Fermi/Large Area Telescope observations of the TeV blazar 1ES 0229 + 200, Mon. Not. R. Astron. Soc. **406**, L70 (2010).
[4] C. Caprini and S. Gabici, Gamma-ray observations of blazars and the intergalactic magnetic field spectrum, Phys. Rev. D **91**, 123514 (2015).
[5] D. Grasso and H. R. Rubinstein, Magnetic fields in the early Universe, Phys. Rep. **348**, 163 (2001).
[6] P. P. Kronberg, Extragalactic magnetic fields, Rep. Prog. Phys. **57**, 325 (1994).
[7] L. M. Widrow, Origin of galactic and extragalactic magnetic fields, Rev. Mod. Phys. **74**, 775 (2002).
[8] M. Giovannini, The magnetized universe, Int. J. Mod. Phys. D **13**, 391 (2004).
[9] A. Kandus, K. E. Kunze, and C. G. Tsagas, Primordial magnetogenesis, Phys. Rep. **505**, 1 (2011).
[10] J. P. Vallée, Magnetic fields in the galactic Universe, as observed in supershells, galaxies, intergalactic and cosmic realms, New Astron. Rev. **55**, 91 (2011).
[11] D. Ryu, D. R. G. Schleicher, R. A. Treumann, C. G. Tsagas, and L. M. Widrow, Magnetic fields in the large-scale structure of the Universe, Space Sci. Rev. **166**, 1 (2012).
[12] R. Durrer and A. Neronov, Cosmological magnetic fields: Their generation, evolution and observation, Astron. Astrophys. Rev. **21**, 62 (2013).
[13] K. Subramanian, The origin, evolution and signatures of primordial magnetic fields, Rep. Prog. Phys. **79**, 076901 (2016).
[14] R. Banerjee and K. Jedamzik, Evolution of cosmic magnetic fields: From the very early Universe, to recombination, to the present, Phys. Rev. D **70**, 123003 (2004).
[15] N. Barnaby, E. Pajer, and M. Peloso, Gauge field production in axion inflation: Consequences for monodromy, non-Gaussianity in the CMB, and gravitational waves at interferometers, Phys. Rev. D **85**, 023525 (2012).
[16] C. Caprini and L. Sorbo, Adding helicity to inflationary magnetogenesis, J. Cosmol. Astropart. Phys. 10 (2014) 056.
[17] M. M. Anber and E. Sabancilar, Hypermagnetic fields and baryon asymmetry from pseudoscalar inflation, Phys. Rev. D **92**, 101501(R) (2015).
[18] K.-W. Ng, S.-L. Cheng, and W. Lee, Inflationary dilaton-axion magnetogenesis, Chin. J. Phys. (Taipei) **53**, 110105 (2015).
[19] T. Fujita, R. Namba, Y. Tada, N. Takeda, and H. Tashiro, Consistent generation of magnetic fields in axion inflation models, J. Cosmol. Astropart. Phys. 05 (2015) 054.
[20] P. Adshead, J. T. Giblin, Jr., T. R. Scully, and E. I. Sfakianakis, Gauge-preheating and the end of axion inflation, J. Cosmol. Astropart. Phys. 12 (2015) 034.
[21] P. Adshead, J. T. Giblin, Jr., T. R. Scully, and E. I. Sfakianakis, Magnetogenesis from axion inflation, J. Cosmol. Astropart. Phys. 10 (2016) 039.
[22] A. Notari and K. Tywoniuk, Dissipative axial inflation, J. Cosmol. Astropart. Phys. 12 (2016) 038.
[23] D. Jiménez, K. Kamada, K. Schmitz, and X. Xu, Baryon asymmetry and gravitational waves from pseudoscalar inflation, J. Cosmol. Astropart. Phys. 12 (2017) 011.
[24] V. Domcke and K. Mukaida, Gauge field and fermion production during axion inflation, J. Cosmol. Astropart. Phys. 11 (2018) 020.
[25] J. R. C. Cuissa and D. G. Figueroa, Lattice formulation of axion inflation. Application to preheating, J. Cosmol. Astropart. Phys. 06 (2019) 002.
[26] Yu. Shtanov, Viable inflationary magnetogenesis with helical coupling, J. Cosmol. Astropart. Phys. 10 (2019) 008.
[27] Y. V. Shtanov and M. V. Pavliuk, Inflationary magnetogenesis with helical coupling, Ukr. J. Phys. **64**, 1009 (2019).
[28] O. O. Sobol, E. V. Gorbar, and S. I. Vilchinskii, Backreaction of electromagnetic fields and the Schwinger effect in pseudoscalar inflation magnetogenesis, Phys. Rev. D **100**, 063523 (2019).
[29] V. Domcke, B. von Harling, E. Morgante, and K. Mukaida, Baryogenesis from axion inflation, J. Cosmol. Astropart. Phys. 10 (2019) 032.
[30] V. Domcke, Y. Ema, and K. Mukaida, Chiral anomaly, Schwinger effect, Euler-Heisenberg Lagrangian, and application to axion inflation, J. High Energy Phys. 02 (2020) 055.
[31] V. Domcke, V. Guidetti, Y. Welling, and A. Westphal, Resonant backreaction in axion inflation, J. Cosmol. Astropart. Phys. 09 (2020) 009.
[32] E. V. Gorbar, K. Schmitz, O. O. Sobol, and S. I. Vilchinskii, Gauge-field production during axion inflation in the gradient expansion formalism, Phys. Rev. D **104**, 123504 (2021).
[33] M. Bastero-Gil and A. T. Manso, Parity violating gravitational waves at the end of inflation, J. Cosmol. Astropart. Phys. 08 (2023) 001.
[34] K. Fukushima, D. E. Kharzeev, and H. J. Warringa, The chiral magnetic effect, Phys. Rev. D **78**, 074033 (2008).
[35] E. V. Gorbar, A. I. Momot, I. V. Rudenok, O. O. Sobol, S. I. Vilchinskii, and I. V. Oleinikova, Chirality production during axion inflation, Ukr. J. Phys. **68**, 717 (2023).
[36] F. Sauter, Über das Verhalten eines Elektrons im homogenen elektrischen Feld nach der relativistischen Theorie Diracs, Z. Phys. **69**, 742 (1931).
[37] W. Heisenberg and H. Euler, Folgerungen aus der Diracschen Theorie des Positrons, Z. Phys. **98**, 714 (1936).
[38] J. Schwinger, On gauge invariance and vacuum polarization, Phys. Rev. **82**, 664 (1951).
[39] G. V. Dunne, Heisenberg-Euler effective Lagrangians: Basics and extensions, in *From Fields to Strings: Circumnavigating Theoretical Physics. Ian Kogan Memorial Collection (3 volume set)*, edited by M. Shifman, A. Vainshtein, and J. Wheater (World Scientific, Singapore, 2005), Vol. 1, pp. 445–522.
[40] R. Ruffini, G. Vereshchagin, and S. S. Xue, Electron-positron pairs in physics and astrophysics: From heavy nuclei to black holes, Phys. Rep. **487**, 1 (2010).

[41] G. S. Bisnovatyi-Kogan, I. A. Kondratiev, and S. G. Moiseenko, Electromagnetohydrodynamics, arXiv:2306.17724.
[42] H. Alfven, Existence of electromagnetic-hydrodynamic waves, Nature (London) **150**, 405 (1942).
[43] B. A. Campbell, S. Davidson, J. R. Ellis, and K. A. Olive, On the baryon, lepton flavor and right-handed electron asymmetries of the Universe, Phys. Lett. B **297**, 118 (1992).
[44] D. Bödeker and D. Schröder, Equilibration of right-handed electrons, J. Cosmol. Astropart. Phys. 05 (2019) 010.
[45] M. H. Thoma, Ultrarelativistic electron-positron plasma, Eur. Phys. J. D **55**, 271 (2009).
[46] M. H. Thoma, Colloquium: Field theoretic description of ultrarelativistic electron-positron plasmas, Rev. Mod. Phys. **81**, 959 (2009).
[47] D. G. Figueroa, J. Lizarrag, A. Urio, and J. Urrestilla, Strong backreaction regime in axion inflation, Phys. Lett. B **131**, 151003 (2023).
[48] V. Domcke, Y. Ema, and S. Sandner, Perturbatively including inhomogeneities in axion inflation, arXiv:2310.0918.
[49] Y. Akrami *et al.* (Planck Collaboration), Planck 2018 results. X. Constraints on inflation, Astron. Astrophys. **641**, A10 (2020).